# NASA Technical Memorandum 78796

# THE EFFECT OF IMPACT DAMAGE AND CIRCULAR HOLES ON THE COMPRESSIVE STRENGTH OF A GRAPHITE-EPOXY LAMINATE



James H. Starnes, Jr., Marvin D. Rhodes and
Jerry G. Williams

October 1978

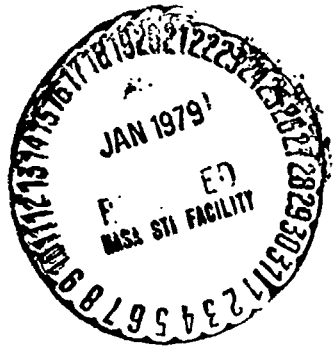


National Aeronautics and
Space Administration

**Langley Research Center**
Hampton, Virginia 23665

# THE EFFECT OF IMPACT DAMAGE AND CIRCULAR HOLES ON THE COMPRESSIVE STRENGTH OF A GRAPHITE-EPOXY LAMINATE

By

James H. Starnes, Jr., Marvin D. Rhodes, and Jerry G. Williams
Langley Research Center

## SUMMARY

An experimental investigation was conducted to determine the effect of low-velocity impact damage and circular holes on the compressive strength of a 48-ply orthotropic graphite-epoxy laminate. Specimens were impacted by 1.27-cm-diameter aluminum spheres with speeds ranging from 52 to 101 m/s. Some specimens were impacted without any applied compressive load and then loaded to failure to determine their residual strength. Other specimens were loaded to a prescribed axial compressive strain and impacted while at that applied load. Loaded specimens that did not fail catastrophically on impact were subsequently loaded to failure to determine their residual strength. Low-velocity impact damage was found to degrade seriously the laminate static compressive strength. Low-strain compression-compression cyclic loading was found to degrade further the compressive strength of impact-damaged specimens. Specimens with circular holes having diameters up to a third of the specimen width were loaded to failure in compression. It was found that circular holes can also degrade the static compressive strength of the laminate. The effects of circular holes and impact damage on the compressive strength of the laminate are compared.

## INTRODUCTION

Advanced composite materials offer an attractive potential for reducing the mass of modern aerospace-vehicle structural components. To achieve this potential, minimum-mass structural designs must be provided that reliably satisfy required design constraints and carry design loads. Reliable designs can be provided only when all failure mechanisms and operational hazards that affect the integrity of a structural component are identified and understood. One operational hazard that can affect the structural integrity of composite compression components is low-velocity impact damage that can occur in service or during maintenance.

Test results from preliminary studies (refs. 1 and 2) indicate that the failure strain of minimum-mass hat-stiffened graphite-epoxy compression panels designed for high strains can be degraded seriously by low-velocity impact damage. Other test results from these studies (ref. 1) indicate that the presence of a small circular hole can also reduce the compressive failure strain of these hat-stiffened panels. The geometric complexity of stiffened panels makes it difficult to isolate and identify the fundamental mechanisms that contribute to the reduction in panel compressive strength. Studies of the effects of low-velocity impact damage on the compressive strength of composite components can be simplified by studying geometrically simpler flat laminates.

This paper presents the results of an exploratory test program to determine the effect of low-velocity impact damage on the compressive strength of a 48-ply orthotropic graphite-epoxy flat laminate. The projectile mass and speeds simulate momenta typical of low-velocity impact hazards that can occur in commercial aircraft service. The laminate selected is typical of designs being proposed for future heavily loaded aircraft wing skins and has extensional and shear stiffness properties similar to existing transport aircraft wing skins designed for an ultimate compressive loading of 2.63 MN/m. Results from tests performed to determine the effect of circular holes on the compressive strength of the same laminate are also presented for comparison with the impact-damage results. The character of the laminate local impact damage is described, the effects of impact damage and circular holes on the static compressive strength of the laminate are discussed, and the effect of cyclic compressive loading on impact-damaged specimens is described.

## TEST SPECIMENS

The specimens tested in this investigation were fabricated from commercially available 450K cure graphite-epoxy preimpregnated tapes. The tapes were made of unidirectional Thornel 300 graphite fibers

preimpregnated with Narmco 5208 epoxy resin and were laid up to form a $(\pm 45/0_2/\pm 45/0_2/\pm 45/0/90)_{2S}$ laminate with 48 plies. These laminates were cured in an autoclave using the manufacturer's recommended procedures. Following cure, the laminates were ultrasonically inspected to establish specimen quality, cut into test specimens, and the ends of the specimens were ground flat and parallel to permit uniform compressive loading. Most specimens were 11.4 cm wide by 24.8 cm long, but a small number were 12.7 cm wide by 25.4 cm long. Circular holes were machined in the center of some of the specimens with diamond impregnated core bits. One side of the specimens was painted white to reflect light so a moire-fringe technique could be used to monitor out-of-plane deformations. The other side of the impact specimens was coated with a brittle lacquer to provide a qualitative measure of impact damage.

The length and width of the specimens were chosen so the fundamental mechanisms that affect compressive strength could be identified and studied without the use of any interior lateral restraints away from the specimen edges. The width of the specimens was selected so the local region influenced by the initial impact damage or holes would be removed from specimen edge effects. Also, the width and length were sized so that a strength failure would be more likely to occur than a buckling failure. The buckling load of the 11.4 cm by 24.8 cm specimens without impact damage or holes was determined, using the BUCLASP 2 computer code (ref. 3), to be 4.40 MN/m at a longitudinal strain of 0.0093. The lamina properties used for the analysis are given in Table 1.

## APPARATUS

Test specimens were loaded in axial compression using a 1.33-MN capacity controlled-displacement hydraulic testing machine for the static load tests and a 0.51-MN capacity controlled-load hydraulic testing machine for the cyclic load tests. The loaded ends of the specimens were clamped by fixtures during testing and the edges were simply supported by knife-edge restraints to prevent the specimen from buckling as a wide column. A typical specimen in the support fixture is shown in figure 1.

Electrical resistance strain gages were used to monitor strains, and direct-current differential transformers were used to monitor axial displacement and displacements normal to the specimen surface. All electrical signals and the correspondings applied loads were recorded on magnetic tape at regular time intervals during the tests. Deflections normal to the specimen surface were also monitored by the moire-fringe technique.

The equipment used to propel the 1.27-cm-diameter aluminum spheres used as impact projectiles is shown schematically in figure 2. Air pressure developed in the reservoir ruptures the diaphragm and allows the compressed air in the reservoir to pass through an orifice and force the projectile down the barrel. An electronic detector at the end of the barrel measures the projectile speed.

An ultrasonic C scan flaw detector was used to measure the extent of impact damage. This detector is a high-resolution commercial instrument that uses a focused pulse-echo type 15-MHz piezoelectric transducer. Both the transducer and the specimens were immersed in a tank of water, and the transducer was mounted to a traversing mechanism to scan the region of interest. This equipment and procedure are described further in reference 4.

## TESTS

The three types of tests conducted during this investigation are: 1) damage characterization tests on specimens to determine the nature of local impact damage; 2) static compressive load tests on control specimens without any impact damage or holes, on specimens subjected to impact damage, and on specimens with circular holes to determine their compressive strength; and 3) cyclic compression-compression tests on impact-damaged and undamaged specimens to determine the effect of low-strain cyclic loading on compressive strength.

### Damage Characterization Tests

Unloaded specimens were supported in the test fixture and subjected to impact damage. The impacted specimens were then inspected both visually and by the ultrasonic C scan procedure. Some of these specimens were cross sectioned through the damaged region and examined microscopically.

### Static Load Tests

Control specimens. - Five control specimens without impact damage or holes were tested in compression to determine their critical compressive loads and strains. Buckling was defined by the load-strain response and strain-reversal techniques. The strain measurements were complemented by the moire-fringe method which provided visual definition of out-of-plane deformations.

Impact-damage specimens. - Four specimens were impacted without any applied compressive load and then loaded in axial compression to determine their residual strength. Eighteen specimens were loaded to prescribed axial compressive strains and impacted while loaded. Specimens that did not fail catastrophically on impact were subsequently loaded to failure to determine their residual strength. During the residual strength tests of these specimens a moire-fringe method was used to observe the out-of-plane deformations. In all impact tests, the projectiles were directed normal to the specimen surface at speeds that ranged from 52 to 101 m/s.

Circular-hole specimens. - Ten specimens, each with a single circular hole in the center, were loaded in compression to failure. The specimens had hole diameters ranging from 0.16 to 3.81 cm (diameter-to-width ratios ranging from 0.014 to 0.333). Small strain gages were used to monitor the strains in the hole region. Gages 1.3 mm wide by 0.8 mm long were used to measure interlaminar normal strains on the surface of the hole and gages 0.3 mm wide by 1.8 mm long were used to measure the inplane axial strains near the hole boundary. Gages 3.2 mm wide by 6.4 mm long were used to measure the inplane axial strains far from the hole. The strain measurements were complemented by the moire-fringe method for out-of-plane deformations.

### Cyclic Load Tests

Three undamaged and four impact-damaged specimens were subjected to low-strain cyclic compression-compression loading to determine its effect on compression strength. These specimens were cycled at a constant amplitude sine wave loading at a rate of 5 Hz to minimize thermal effects. The growth of the damaged region was observed visually.

## RESULTS AND DISCUSSION

### Damage Characterization Tests

Unloaded specimens were subjected to impact to determine the character of local impact damage. Photographs of the back surfaces of two specimens impacted at 58 and 95 m/s are shown in figure 3. The light colored regions shown in the figure are regions where the brittle lacquer spalled b' ind the impact location. Radial cracks in the brittle lacquer near the spalled region are also visible. Both the radial cracks and the spalled region indicate that significant deformations have occurred locally due to impact. There is no visible damage to the graphite epoxy on the back surface of the specimen impacted at 58 m/s, but some local surface cracks in the graphite epoxy are visible on the back surface of the specimen impacted at 95 m/s. There is no visible front-surface damage at the impact location of either specimens. Photographs of ultrasonic C scans of the damaged regions of these specimens are shown in figure 4 with the same scale used in figure 3. Each pass of the transducer is represented by a light colored line in the figure. The size of the dark regions indicates the extent of damage in both specimens as a result of impact. The damaged region of the specimen impacted at 58 m/s is smaller and more elongated in the 0° direction than the specimen impacted at 95 m/s. Ultrasonic inspection also indicates that the spalled brittle lacquer provides a qualitative approximation to the size of the damaged region. Photomicrographs of a cross section normal to the 0° fibers through the damaged region of the specimens are shown in figure 5. The photomicrograph of the specimen impacted at 58 m/s shows only a small amount of intraply

cracking and delamination in the impact region. The photomicrograph of the specimen impacted at 95 m/s shows extensive intraply matrix cracking and delamination in the impact region. This cracking and delamination extends 3.4 cm across the width of the specimen. This extensive region of delamination has changed the 48-ply orthotropic laminate into a number of thinner sublaminates in the damaged region that are likely to be anisotropic, thus reducing local stiffnesses and causing local anisotropic coupling. The ultrasonic C scans in figure 4 and the photomicrographs in figure 5 indicate that the projectile used in this study causes substantial internal damage to the laminate with no visible external damage at the impact site for speeds up to approximately 100 m/s.

## Static Load Tests

Control specimens. - The results of the control-specimen tests are presented in Table 2. Moire-fringe patterns indicated that specimens N1, N3, N4 and F1 buckled into two axial half waves and one transverse half wave. Specimen N2 failed near an end fixture after back-to-back strain gages indicated the onset of bending. Specimens N1 and F1 failed near an end fixture just after buckling was indicated by the moire-fringe patterns. The loading of specimens N3 and N4 was stopped before failure, but after the moire-fringe patterns indicated buckling. These specimens (N3 and N4) were subsequently used for impact-damage tests. The differences in the control-test results were caused by local stress concentrations that developed in small gaps between the end fixtures and edge supports when out-of-plane deformations occurred. When out-of-plane deformations occurred, the end fixtures and edge supports moved relative to one another causing the specimens to fail in one of these gaps. Also, small surface irregularities could affect the tightness of fit of the edge supports and introduce different degrees of edge-support flexibility. Even though there is scatter in the results presented in Table 2, these results confirm that the specimens buckle at strains high enough to assure that strength-controlled failures are likely to occur when there is impact damage or a hole in a specimen.

Impact-damage specimens. - The results of the impact-damage tests are presented in Table 3, and the effect of projectile speed on specimens impacted while loaded to a prescribed axial strain is shown in figure 6. The applied axial strains of the loaded specimens that failed catastrophically on impact are represented by the filled circles in figure 6 and the applied strains of the specimens that did not fail catastrophically on impact are represented by open circles. The results from Table 2 for the undamaged control specimens are shown on the ordinate as open circles for comparison, and the projectile kinetic energy is also shown on the abscissa for reference. The dashed curve in figure 6 represents a lower bound or catastrophic failure threshold separating results of specimens that failed on impact from those that did not. The trend of this catastrophic failure threshold indicates that the compressive strength of these loaded impact specimens is seriously degraded with increasing projectile speed with most of the degradation having occurred by about 80 m/s. A typical failed specimen is shown in figure 7.

The effect of projectile speed on the residual strength of all specimens that did not fail catastrophically on impact is shown in figure 8. The open circles in figure 8 indicate the axial strain the specimens were carrying at the moment of impact, and the filled circles represent the strain at failure measured during residual strength tests. Each open circle in figure 8 has a corresponding filled circle directly above it, and the difference in strain between two corresponding circles represents the additional applied axial strain carried by a damaged specimen. Results from Table 2 for the control tests are shown on the ordinate of figure 8 as filled circles for comparison, and the projectile kinetic energy is shown on the abscissa for reference. The catastrophic failure threshold curve from figure 6 is also shown on figure 8 as a dashed curve for comparison. Specimens impacted in the 50 to 60 m/s range that did not fail catastrophically on impact have residual strengths between 0.0104 and 0.0087 axial strain which is on the same order as the undamaged control specimens. Three of the four specimens impacted in this speed range failed near an end fixture and the fourth failed through the impact site. Specimens impacted in the 80 to 100 m/s range have residual strengths that are only between 0.0044 and 0.0034 axial strain. Specimens impacted in this speed range with no applied axial load fail at higher values of applied axial strain than those impacted while loaded axially and, consequently, have higher residual strengths. Furthermore, a comparison of the residual strength results of figure 8 with the catastrophic failure threshold from figure 6 indicates that catastrophic failure of specimens impacted while loaded axially occurs at applied strains that are slightly below the residual strength results of specimens impacted without applied axial load in the 80 to 100 m/s projectile speed range. However, in the 50 to 60 m/s projectile speed range the catastrophic failure threshold strains for specimens impacted while loaded axially is on the order of 0.002 to 0.003 less strain than the residual strength results for specimens impacted without applied axial load. This difference in loaded and unloaded impact test results indicates that there is an interaction or coupling between the applied inplane load and the local deformations associated with impact. The existence of this coupling is also supported by ultrasonic C scan and cross sectional photomicrograph data. Ultrasonic C scans made before the residual strength tests indicate that damage due to impact for the specimens impacted between 50 and 60 m/s is local and approximately circular with 1.8 to 2.5 cm diameters. These specimens had no visible front- or back-surface damage. Visual inspection of the specimens impacted between 80 and 100 m/s indicated that some local 45° cracks existed on the back surfaces but no front-surface damage was evident. Ultrasonic C scans of these specimens indicate that the local damage due to impact is elliptical. For the specimens impacted without any applied axial strain, the size of the ellipse ranges from 3.6 cm wide by 4.3 cm long to 4.6 cm wide by 5.8 cm long with semimajor axes oriented in the axial direction. For specimen N20, which was impacted at 100 m/s while loaded by an applied axial strain of 0.0027, the ellipse is 5.1 cm wide by 3.8 cm long with its semimajor axis oriented in the transverse direction which is a change in orientation of 90° from the specimens impacted without applied axial strain. Instead of determining its residual strength, specimen N20

was cross sectioned through the local impact-damaged region to determine the character of the damage. Photomicrographs of the damaged region show extensive local delamination and intraply matrix cracking that extends 4.6 cm across the width of the specimen and is similar to that shown in figure 5b. This 1.2 cm increase in delamination width over the 3.4 cm delamination width of the unloaded damage characterization specimen impacted at 95 m/s indicates there is coupling between the applied axial load and local deformation due to impact. This coupling may account for the lower residual strength of the specimens impacted while loaded axially.

Photographs of successive moire-fringe patterns from the residual strength test of specimen N7 are shown in figure 9. Specimen N7 was impacted at 91 m/s with no applied axial load. The photograph in figure 9a shows the moire-fringe pattern of the damaged region at 48 percent of the specimen residual strength. The small light colored circular region in the center of the specimen is the impact site which is beginning to deform out-of-plane. This deformation is the first observable response of the damaged region to the applied axial load. Subsequent moire-fringe patterns (figs. 9b and 9c) represent local buckling of the impact-damaged region that grows laterally as the applied load is increased. The photograph in figure 9d shows the failed specimen with the damage propagated laterally across the specimen in the same manner as the example shown in figure 7. Examination of the failed specimen removed from the test fixture confirmed that the damage propagated laterally and was confined axially to the region indicated in figure 9d.

Circular-hole specimens. - Axial strains $\varepsilon_x$ measured in the vicinity of four different diameter holes are shown in figure 10 normalized by the applied axial strain $\varepsilon_a$ of 0.0026. The seven strain gages used to measure these strains were distributed along a line indicated by the y-axis in the sketch in figure 10. One of these gages was located on the surface of the hole edge and the other six were located at 0.16, 0.32, 0.64, 1.27, 1.91 and 2.54 cm from the hole edge. The gage locations $y$ in figure 10 are normalized by the hole diameter $D$. The ratio of measured strain to applied strain for the four holes is slightly higher than the calculated value of 3.31 for the ratio of maximum strain to applied strain for an infinitely wide orthotropic plate determined from reference 5. Even though the results indicate some finite-width effects for these 11.4 cm wide specimens, the strains near the hole decrease rapidly to the value of the applied strain as the distance from the holes increases. In addition to the local inplane axial strains, through-the-thickness or interlaminar normal strains were measured at points on the free edge of the larger holes with strain gages oriented parallel to the hole axis. Typical data measured by three of these gages for a 1.91-cm-diameter hole are shown in figure 11 as a function of applied load. The applied axial strain is also shown for comparison. The location of these three gages is represented by the small filled circles in the sketch in figure 11 and the gages are labeled as gages 1, 2 and 3. Gage 1 indicates a tensile strain between 20 and 30 percent of the applied axial strain. Gage 3 indicates a compressive strain of about 38 percent of the applied strain.

Gage 2 indicates a small compressive strain of about 8 percent of the applied axial. Near failure gages 1 and 2 become very erratic. The combination of the high inplane compressive strain and the high interlaminar tensile strain near the hole causes local delamination to occur and propagate across the specimen as the applied load is increased. The erratic behavior of gages 1 and 2 near failure is probably due to local delamination in the hole region.

A series of photographs of the propagating moire-fringe patterns for a specimen with a 1.91-cm-diameter hole is shown in figure 12 for increasing values of applied load. Figure 12a shows a photograph of the specimen loaded to 92.8 percent of the ultimate failure load and the absence of moire fringes indicates there are no out-of-plane deformations evident. At a slightly higher load (fig. 12b) a small out-of-plane deformation region developed at the left edge of the hole. These results, along with the strain gage results in the hole region and direct visual observations, indicate that a local delamination has developed near the hole. A second local delamination developed at the right edge of the hole (fig. 12c) after another slight increase in applied load. These delaminated regions continued to propagate, first in short discrete increments (fig. 12d), and then rapidly at the failure load (fig. 12e). The failed specimen shown in figure 12e was cut along an axial line passing through the center of the hole. A photograph of the cross section of the specimen in figure 13 shows many local delaminations through the thickness of the laminate. These delaminations extend completely across the specimen width but only extend a short distance in the axial direction.

The test results for the hole specimens are presented in Table 1, and the effect of hole diameter on failure strain is shown in figure 14. Results from Table 2 for the control tests are also shown on the ordinate of figure 14 for comparison. Specimen H1 with the 0.16 cm diameter hole failed near an end support fixture like the control specimens and at about the same strain. Thus, local effects associated with the test fixture were more critical than those of the hole for this specimen. All other specimens failed in the hole region at applied strains that decrease as the hole diameter increases. The catastrophic failure threshold from figure 6 for specimens impacted at 100 m/s is also shown in figure 14 as a dashed line for comparison with the hole results.

A comparison of the hole results with the impact-damage results indicates that, for the projectile used in this investigation, impact speeds of about 100 m/s degrade the laminate compressive failure strain about 0.001 more than the largest hole studied. Impact speeds of about 50 to 60 m/s have little effect on the compressive failure strain; even though ultrasonic C scan inspection indicates interior damage (fig. 4a). However, a specimen loaded axially during impact at a speed of 50 to 60 m/s will fail at about the same strain as a specimen with a 0.64 cm diameter hole. As indicated by a comparison of figures 9a and 12b, the load at which delamination occurs in specimens with holes and impact damage usually differs. Delamination can occur due to impact regardless of the applied load, and the delamination may not be evident from a

visual inspection of the impacted surface. Sublaminates formed by impact-induced delamination can buckle locally causing the delamination to propagate when the specimen is loaded. For a specimen with a hole, delamination is not initiated until the applied axial load is high enough to cause a local failure at the hole boundary. Thus, the loads necessary to propagate delaminations could be different for specimens with impact damage or holes, and the use of hole-strength data to predict impact-damage strength may be questionable.

## Cyclic Load Tests

The test parameters and results for the cyclic-load specimens are presented in Table 5. Three specimens without impact damage were subjected to at least one million cycles with maximum applied axial strains of 0.003, 0.004 and 0.005 respectively. These specimens showed no evidence of any change in stiffness due to the cyclic loading and there was no evidence of interior damage from ultrasonic C scan inspection due to cyclic loading.

Four unloaded specimens were impacted with projectiles with speeds of about 100 m/s and then loaded cyclically with various maximum applied strain levels. The initial impact damage was similar to that of the other specimens impacted at this speed and reported in the previous section. Three of the four impact-damaged specimens failed at or less than 173000 cycles; the specimen with the lowest maximum applied strain did not fail before the test was terminated at a million cycles. The maximum cyclic strains and the static failure strains for specimens impacted without any applied axial load are shown in figure 15. The open circles on the abscissa represent the impact speeds for the unloaded impact specimens and the filled circles represent their residual failure strain. The results from Table 2 for the control specimens are shown on the ordinate as filled circles for comparison. The open square in figure 15 represents a test where the load was cycled a million times without failure. The filled squares represent tests where failure occurred within a million cycles. The maximum cyclic strains that failed these specimens are below the residual strength of the corresponding statically loaded specimens. During cyclic loading the impact-induced delaminated region buckled cyclically out of plane. Specimen C6 failed by progressive delamination that started to grow after about 140000 cycles. The growth of the delaminated region was monitored by observing the changes in the spalled region of the brittle lacquer on the specimen as shown by the photographs in figure 16. Changes in the spallation pattern of the brittle lacquer provided a direct way to monitor visually the growth of subsurface damage. At the conclusion of this test the specimen was inspected ultrasonically, and the results indicated that the failure was confined to the spalled region shown in Figure 16c.

The impact damage in specimen C4 did not grow after a million cycles and the specimen was statically loaded to failure to determine its

residual strength. The specimen failed through the impact-damaged region at an applied strain of 0.0034 which is on the same order as the statically loaded impact specimens. These preliminary data suggest that cyclic compression loading of an impact-damaged laminate may further degrade the residual strength.

## CONCLUDING REMARKS

An experimental investigation was conducted to determine the effect of low-velocity impact damage and unloaded circular holes on the compressive strength of a 48-ply orthotropic laminate made of unidirectional Thornel 300 graphite fibers preimpregnated with Narmco 5208 epoxy resin. Forty two specimens were fabricated from unidirectional tapes laid up to form a $(\pm 45/0_2/\pm 45/0_2/\pm 45/0/90)_{2S}$ laminate and were tested by either static or cyclic compression.

Specimens were impacted by a 1.27-cm-diameter aluminum sphere with speeds ranging from 52 to 101 m/s. Some specimens were impacted without any applied compressive load and then loaded to failure to determine their residual strength. Other specimens were loaded to a prescribed axial compressive strain and impacted while at that applied load. Loaded specimens that did not fail catastrophically on impact were inspected for damage and subsequently loaded to failure to determine their residual strength. For the range of projectile speeds considered low-velocity impact damage caused extensive local interior damage in the laminate in the form of matrix cracking and delamination without causing any visible external damage at the impact site. Low-velocity impact damage can seriously degrade the static compressive strength of the laminate. Specimens that fail at axial strains above 0.008 in the undamaged condition can fail at strains as low as 0.0031 when impacted at 100 m/s. The compressive strength of specimens impacted while loaded axially is lower than specimens that were impacted without any applied axial load. This difference indicates there is a coupling between the local deformation due to impact and the applied compressive strain. Once local interior damage occurs, it can propagate across the specimen as the applied load is increased and fail the specimen.

Cyclic compression-compression loading can further degrade the compression strength of impact-damaged specimens. Specimens impacted at 100 m/s failed after less than a million cycles for maximum applied axial cyclic strains below the static residual strength values.

Circular holes can also reduce the static compressive strength of the laminate. The failure strain of the specimens decreased as the hole diameter was increased. Specimens impacted at speeds of 100 m/s failed at lower applied axial strains than the specimen with the largest hole diameter tested. A distinction between the effects of holes and impact damage is the load at which delamination occurs. Impact-induced delamination occurs on impact for sufficiently high

impact speeds regardless of the applied strain level. For holes, delamination occurs near the hole boundary when the applied strain is sufficiently high to cause local failure due to local strain concentrations. Because of this difference between holes and impact damage, the use of hole-strength data to predict impact-damage strength may be questionable when high compressive strains must be carried.

Langley Research Center
National Aeronautics and Space Administration
Hampton, VA 23665
October 30, 1978

## REFERENCES


1. Rhodes, Marvin D.; Williams, Jerry G.; and Starnes, James H., Jr.: Effect of Low-Velocity Impact Damage on the Compressive Strength of Graphite-Epoxy Hat-Stiffened Panels. NASA TN D-8411, 1977.

2. Rhodes, Marvin D.; Williams, Jerry G.; and Starnes, James H., Jr.: Effect of Impact Damage on the Compression Strength of Filamentary-Composite Hat-Stiffened Panels. The Society of Advanced Materials and Process Engineering Series, Vol. 23, "Selective Application of Materials for Products and Energy," SAMPE, pp. 300-319, 1978.

3. Viswanathan, A. V.; and Tamekuni, M.: Elastic Buckling Analysis for Composite Stiffened Panels and Other Structures Subject to Biaxial Inplane Loads. NASA CR-2216, 1973.

4. Platt, Robert J., Jr.; and Thurston, Lewis B., Jr.: Holographic and Ultrasonic Detection of Bond Flaws in Aluminum Panels Reinforced with Boron-Epoxy. NASA TN D-7632, 1974.

5. Lekhnitskii, S. G.: Theory of Elasticity of an Anisotropic Elastic Body. Holden-day, Inc., 1963.

TABLE 1- Lamina properties used in buckling analyses.

| | |
|---|---|
| Cured ply thickness, mm | 0.14 |
| Longitudinal modulus, GPa | 131.0 |
| Transverse modulus, GPa | 13.0 |
| Shear modulus, GPa | 6.4 |
| Major Poisson's ratio | 0.38 |

TABLE 2- Results of control specimen tests.

| Specimen[a] | Thickness, cm | Load, kN | Maximum applied strain |
|---|---|---|---|
| N1 | 0.70 | 427 | 0.0089 |
| N2 | 0.70 | 403 | 0.0082 |
| N3 | 0.70 | 495 | 0.0105 |
| N4 | 0.70 | 448 | 0.0095 |
| F1 | 0.68 | 467 | 0.0083 |

[a]Specimen dimension code: N = 11.4 cm by 24.8 cm; F = 12.7 cm by 25.4 cm.

TABLE 3- Test results for impact-damaged specimens.

| Specimen[a] | Thickness, cm | Load conditions at impact: Applied strain | Load conditions at impact: Load, kN | Impact data: Projectile speed, m/s | Impact data: Interior damage size in centimeters | Residual strength: Applied strain | Residual strength: Load, kN |
|---|---|---|---|---|---|---|---|
| N5 | 0.67 | 0. | 0. | 60 | Data not available | 0.0087 | 428 |
| N6 | .70 | 0. | 0. | 79 | 3.6 wide by 4.6 long | .0044 | 226 |
| N7 | .70 | 0. | 0. | 91 | 3.6 wide by 4.3 long | .0039 | 189 |
| N8 | .67 | 0. | 0. | 93 | 4.6 wide by 5.8 long | .0039 | 191 |
| N9 | .67 | .0071 | 363 | 52 | Failed on impact | ... | ... |
| N3 | .70 | .0042 | 220 | 53 | 1.8 diameter circle | .0104 | 495 |
| N4 | .70 | .0054 | 274 | 58 | 2.3 diameter circle | .0095 | 449 |
| N10 | .70 | .0062 | 310 | 56 | 2.5 diameter circle | .0102 | 479 |
| N11 | .70 | .0069 | 346 | 60 | Failed on impact | ... | ... |
| N12 | .70 | .0041 | 209 | 84 | Failed on impact | ... | ... |
| N13 | .70 | .0047 | 241 | 95 | Failed on impact | ... | ... |
| N14 | .70 | .0061 | 308 | 99 | Failed on impact | ... | ... |
| N15 | .67 | .0027 | 144 | 100 | Data not available | .0034 | 155 |
| N16 | .67 | .0030 | 161 | 99 | Failed on impact | ... | ... |
| N17 | .67 | .0033 | 174 | 98 | Failed on impact | ... | ... |
| N18 | .67 | .0036 | 191 | 98 | Failed on impact | ... | ... |
| N19 | .67 | .0039 | 206 | 100 | Failed on impact | ... | ... |
| N20 | .67 | .0027 | 143 | 100 | 5.1 wide by 3.8 long | Residual strength not determined | |
| F2 | .68 | .0036 | 205 | 76 | Failed on impact | ... | ... |
| F3 | .69 | .0032 | 179 | 80 | Data not available | .0035 | 194 |
| F4 | .67 | .0031 | 178 | 89 | Failed on impact | ... | ... |
| F5 | .67 | .0027 | 156 | 88 | Data not available | .0031 | 173 |

[a]Specimen dimension code: N = 11.4 cm by 24.8 cm; F = 12.7 cm by 25.4 cm.

TABLE 4- Test results for circular hole specimens.

| Specimen | Thickness, cm | Hole diameter, cm | Failure strain | Failure load, kN |
|---|---|---|---|---|
| H1 | 0.065 | 0.16 | 0.0088 | 471 |
| H2 | 0.070 | 0.64 | 0.0070 | 343 |
| H3 | 0.069 | 1.27 | 0.0057 | 297 |
| H4 | 0.069 | 1.91 | 0.0045 | 252 |
| H5 | 0.070 | 1.91 | 0.0045 | 250 |
| H6 | 0.069 | 2.54 | 0.0045 | 265 |
| H7 | 0.070 | 2.54 | 0.0044 | 228 |
| H8 | 0.069 | 3.18 | 0.0040 | 201 |
| H9 | 0.069 | 3.81 | 0.0039 | 190 |
| H10 | 0.069 | 3.81 | 0.0039 | 190 |

TABLE 5- Test results for cyclic compression-compression loaded specimens.

| | Test conditions | | | Results | |
|---|---|---|---|---|---|
| Specimen | Projectile impact speed,m/s | Maximum applied strain | R[a] | Number of cycles in millions | Response |
| C1 | 0 | 0.0030 | 35.9 | 1.73 | No damage, test terminated |
| C2 | 0 | 0.0040 | 45.8 | 1.0 | No damage, test terminated |
| C3 | 0 | 0.0050 | 58.3 | 1.0 | No damage, test terminated |
| C4 | 100 | 0.0020 | 24.0 | 1.0 | No damage growth, test terminated |
| C5 | 101 | 0.0022 | 26.0 | 0.042 | Failed during test |
| C6 | 96 | 0.0025 | 28.8 | 0.173 | Slow delamination growth to failure |
| C7 | 96 | 0.0026 | 31.3 | 0.016 | Failed during test |

[a]R is the ratio of minimum to maximum applied loads.

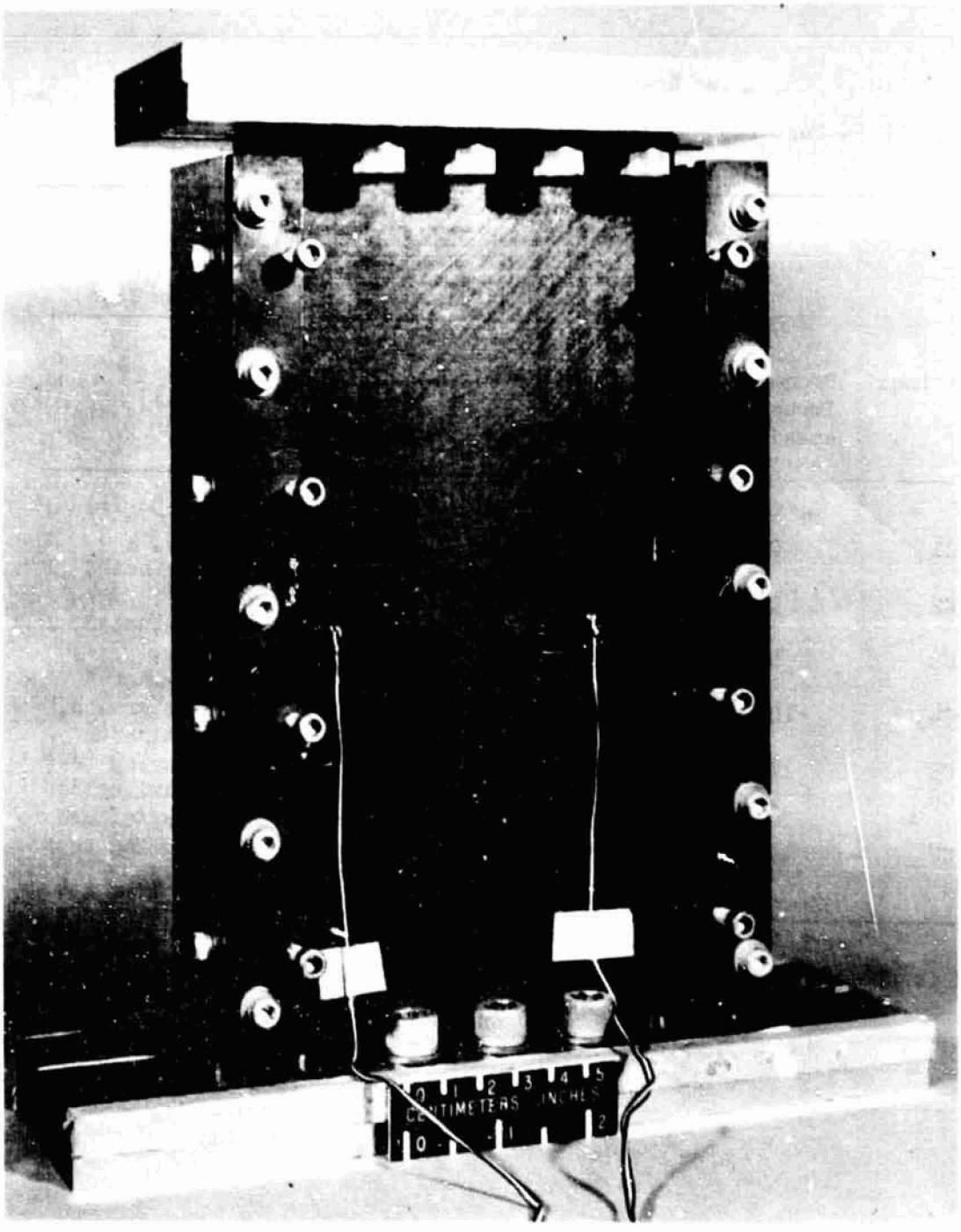


Figure 1. - 48-ply graphite-epoxy specimen in test fixture.

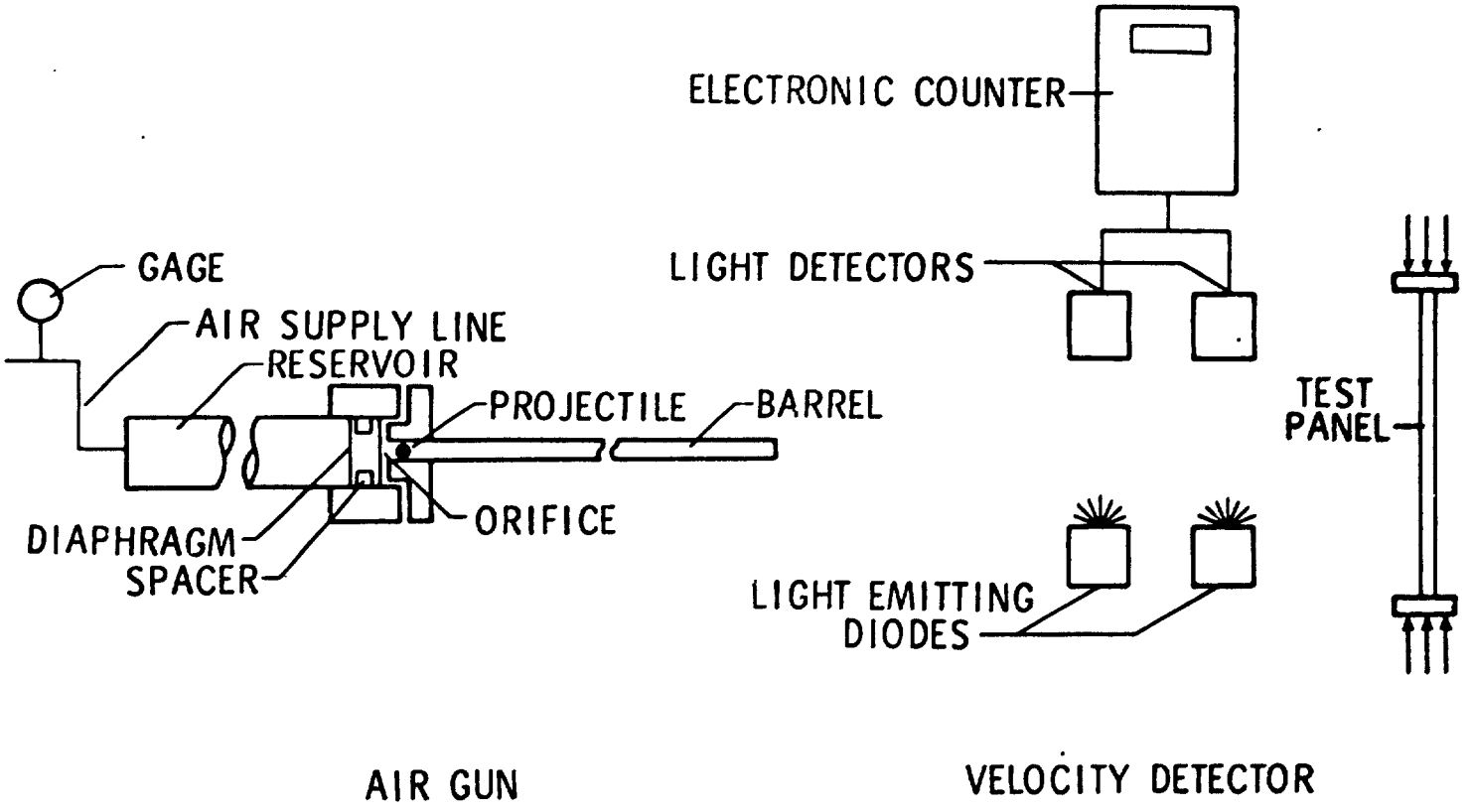


Figure 2. - Schematic drawing of air gun and velocity detector.

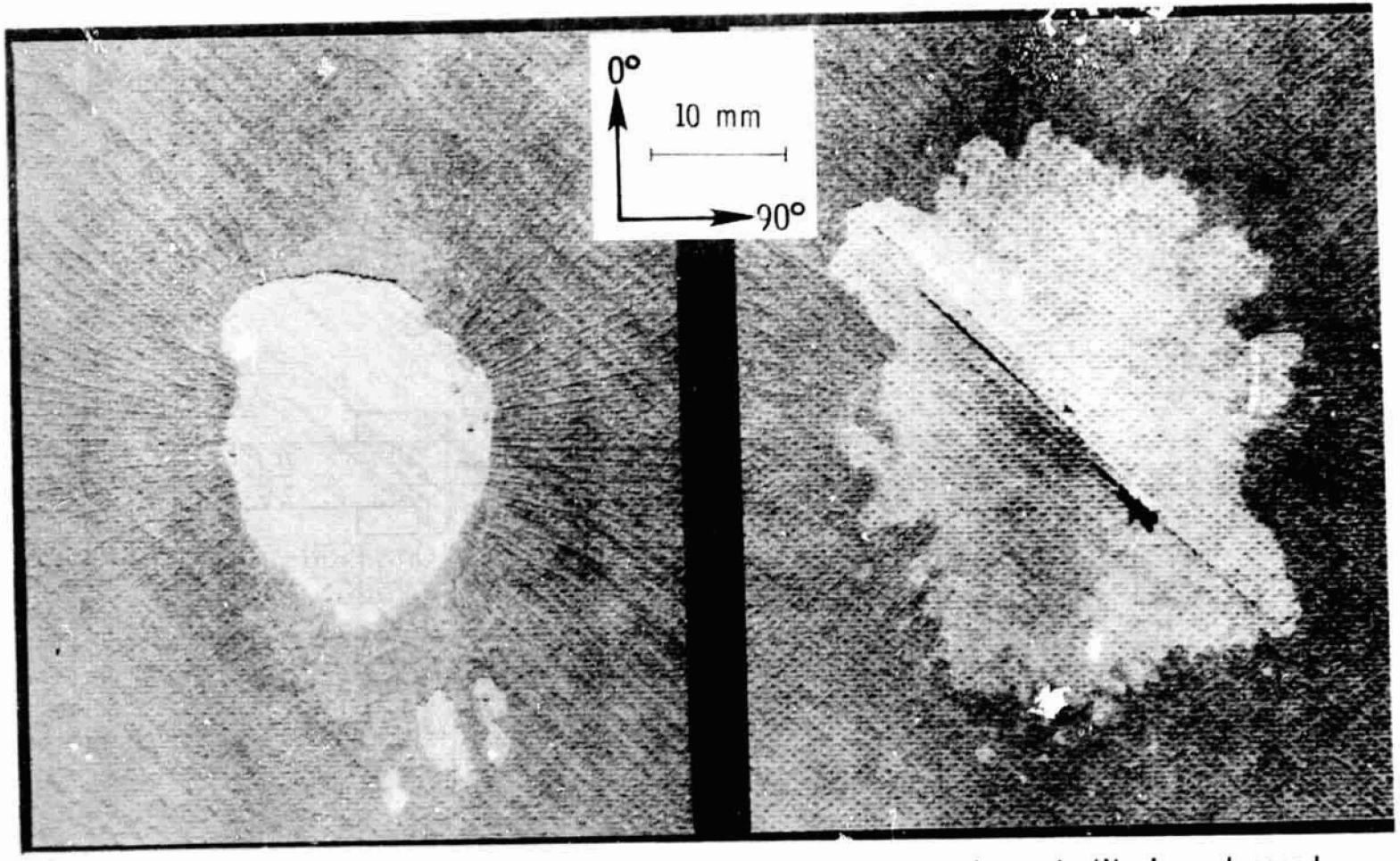


(a) 58 m/s projectile impact speed.

(b) 95 m/s projectile impact speed.

Figure 3.- Brittle-lacquer spalling pattern on impact-specimen back surface.

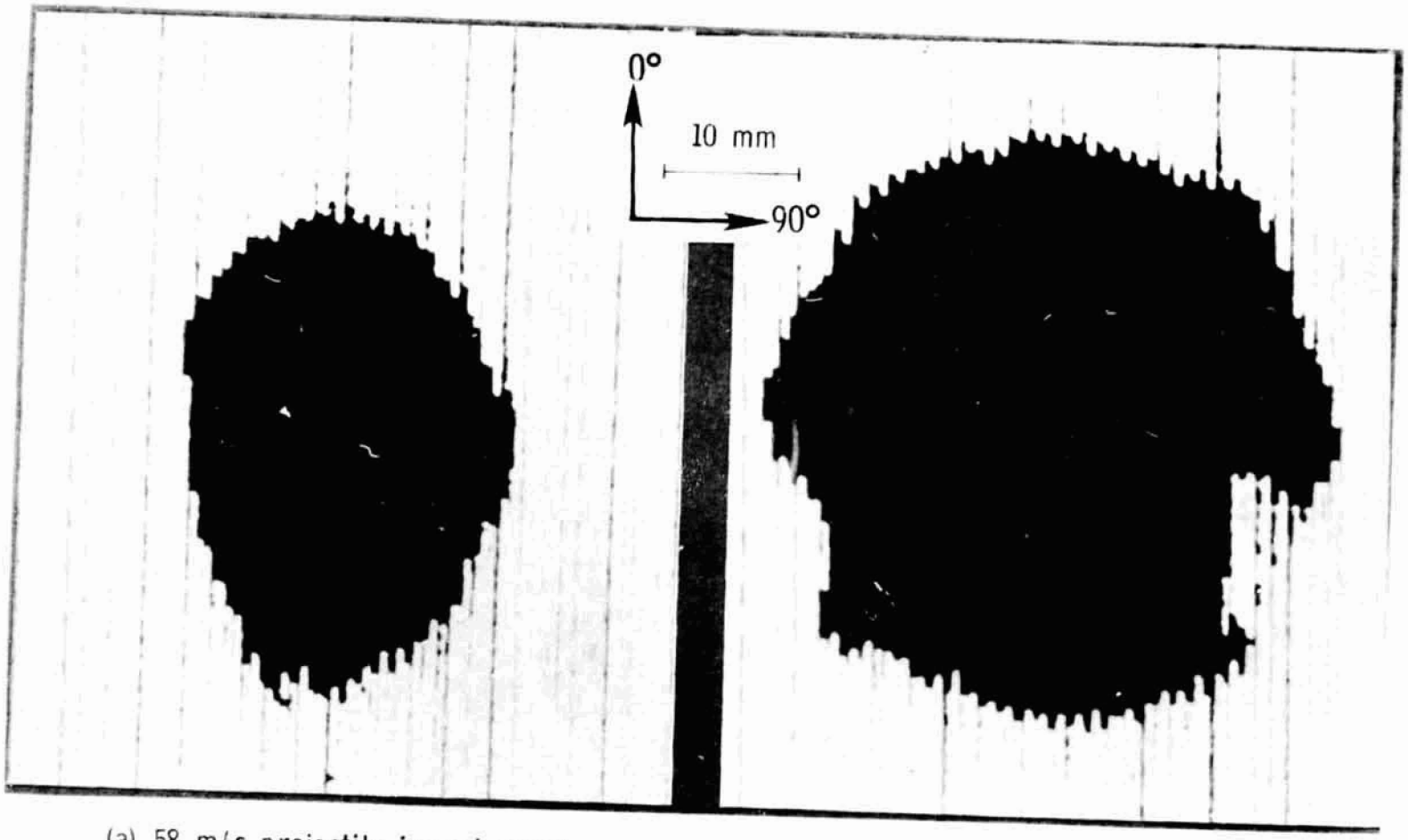


(a) 58 m/s projectile impact speed.

(b) 95 m/s projectile impact speed.

Figure 4. - Ultrasonic C scan of impact site.

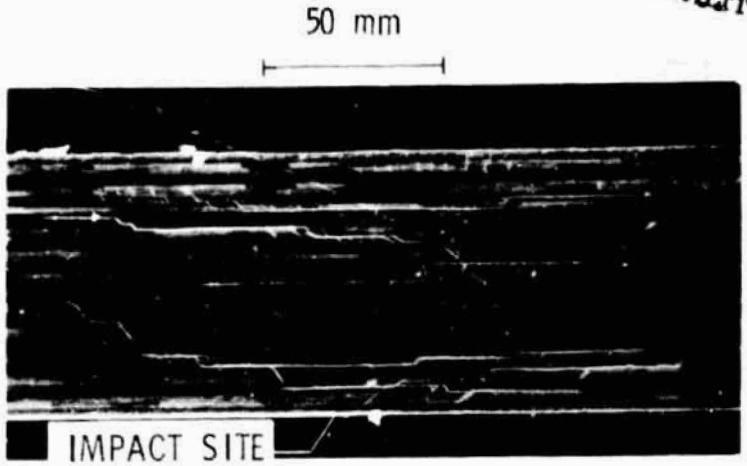


(a) 58 m/s projectile impact speed.

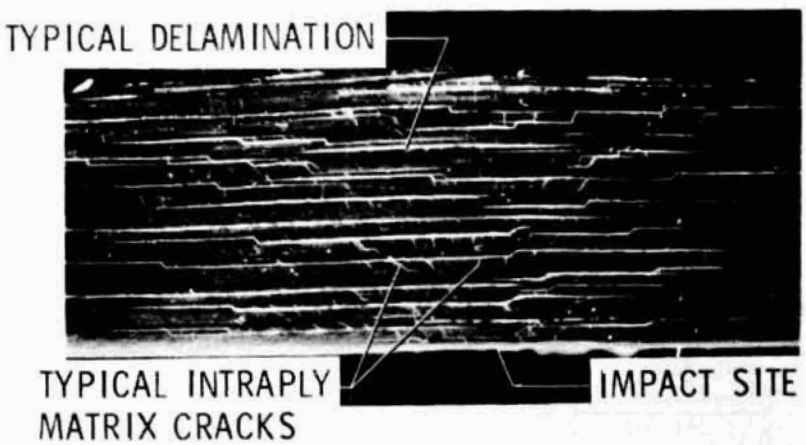


(b) 95 m/s projectile impact speed.

Figure 5. - Photomicrographs of cross sections through the impact site normal to the $0^{0}$ fibers.

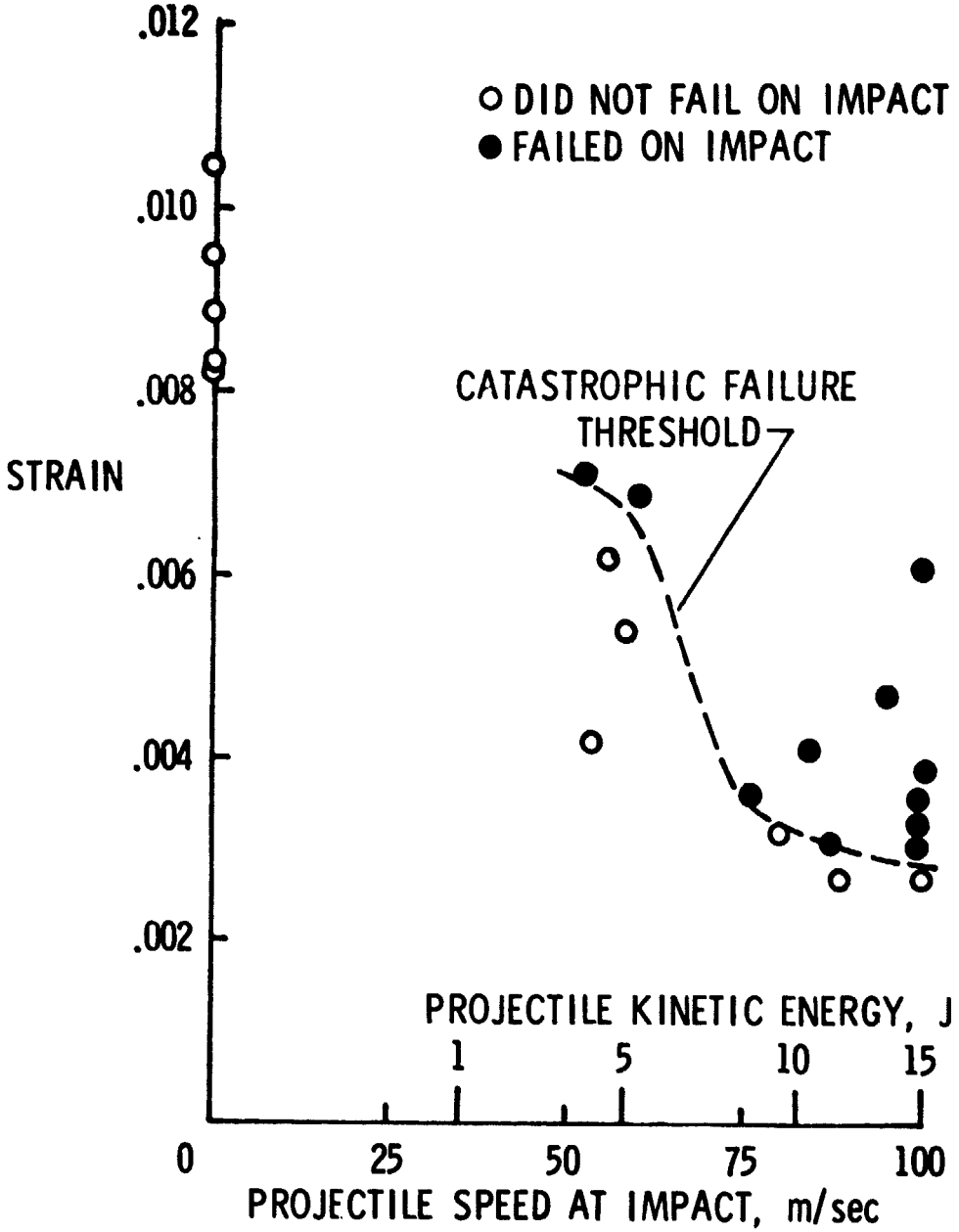


Figure 6.- Effect of projectile speed on catastrophic failure strain.


Figure 7. - Typical failed impact-damaged specimen.

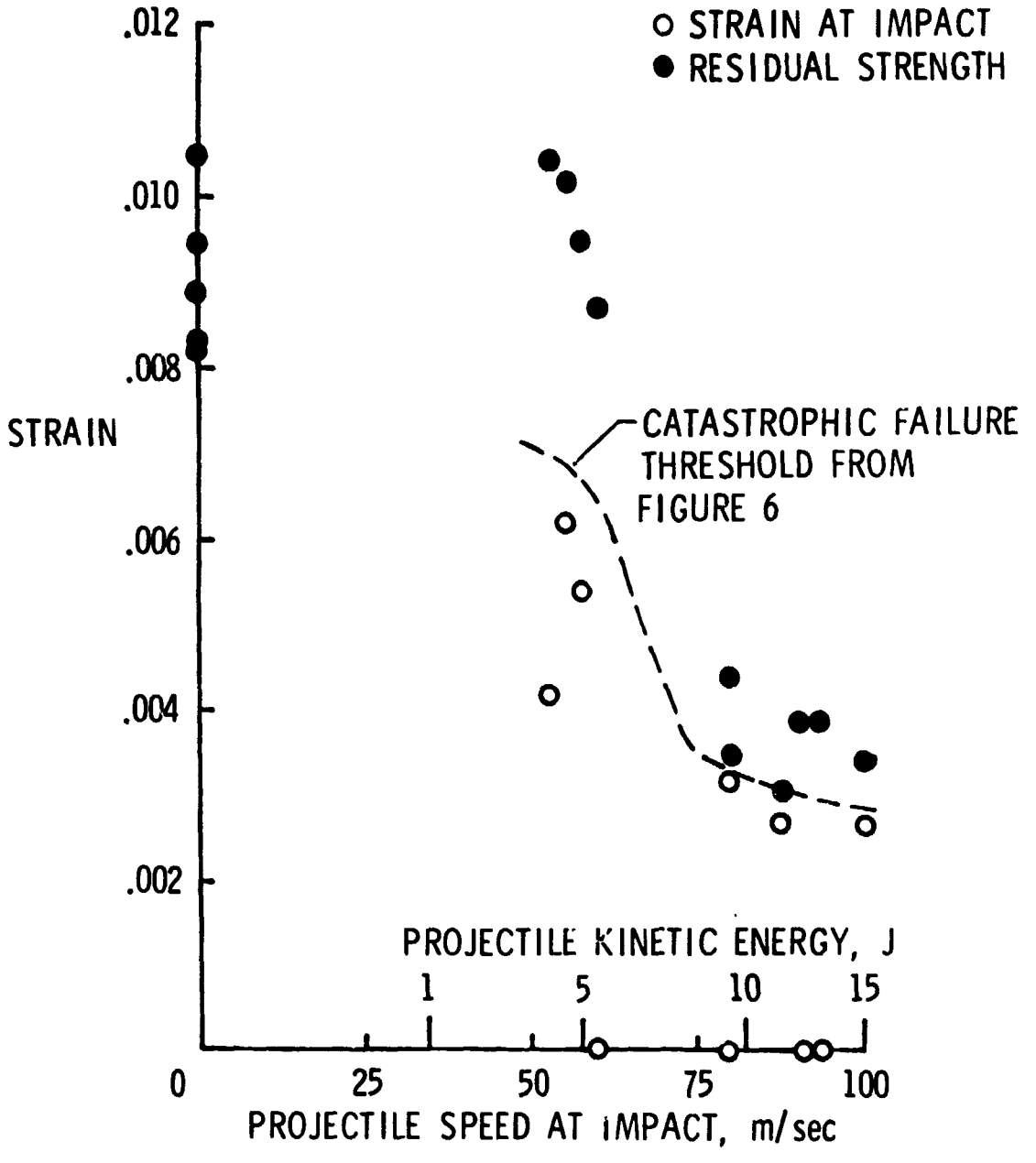


Figure 8. - Effect of projectile speed on residual strength.

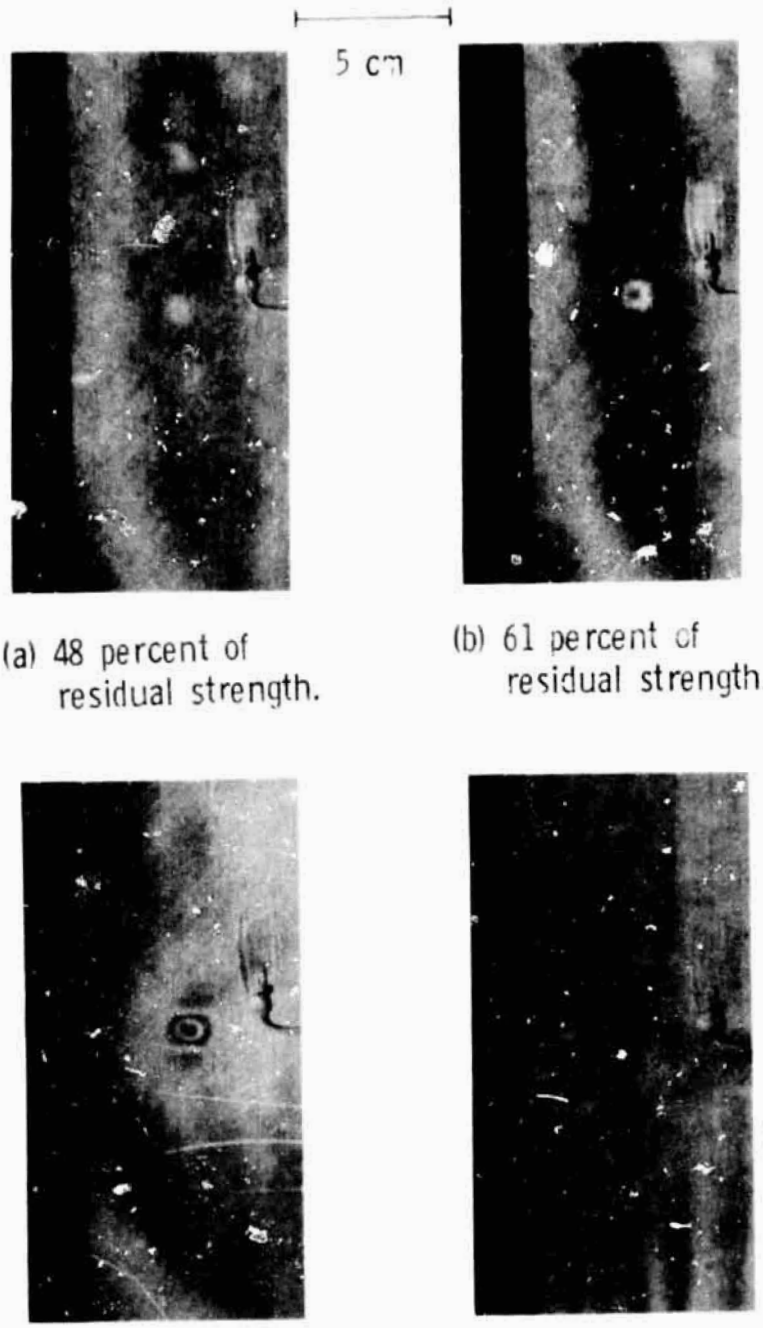


(a) 48 percent of residual strength.

(b) 61 percent of residual strength.

(c) 98 percent of residual strength.

(d) Failed specimen.

Figure 9. - Moire-fringe patterns during residual-strength test of an impact damaged specimen.

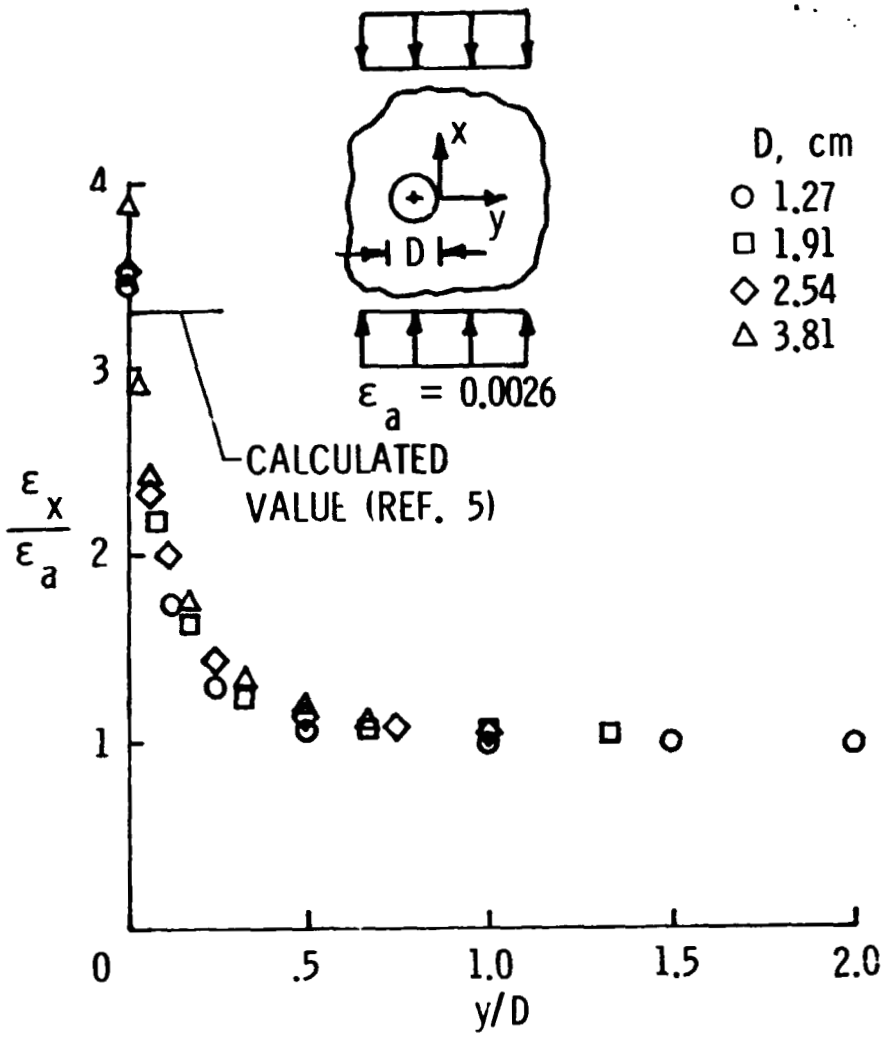


Figure 10. - Strain concentration in hole region.

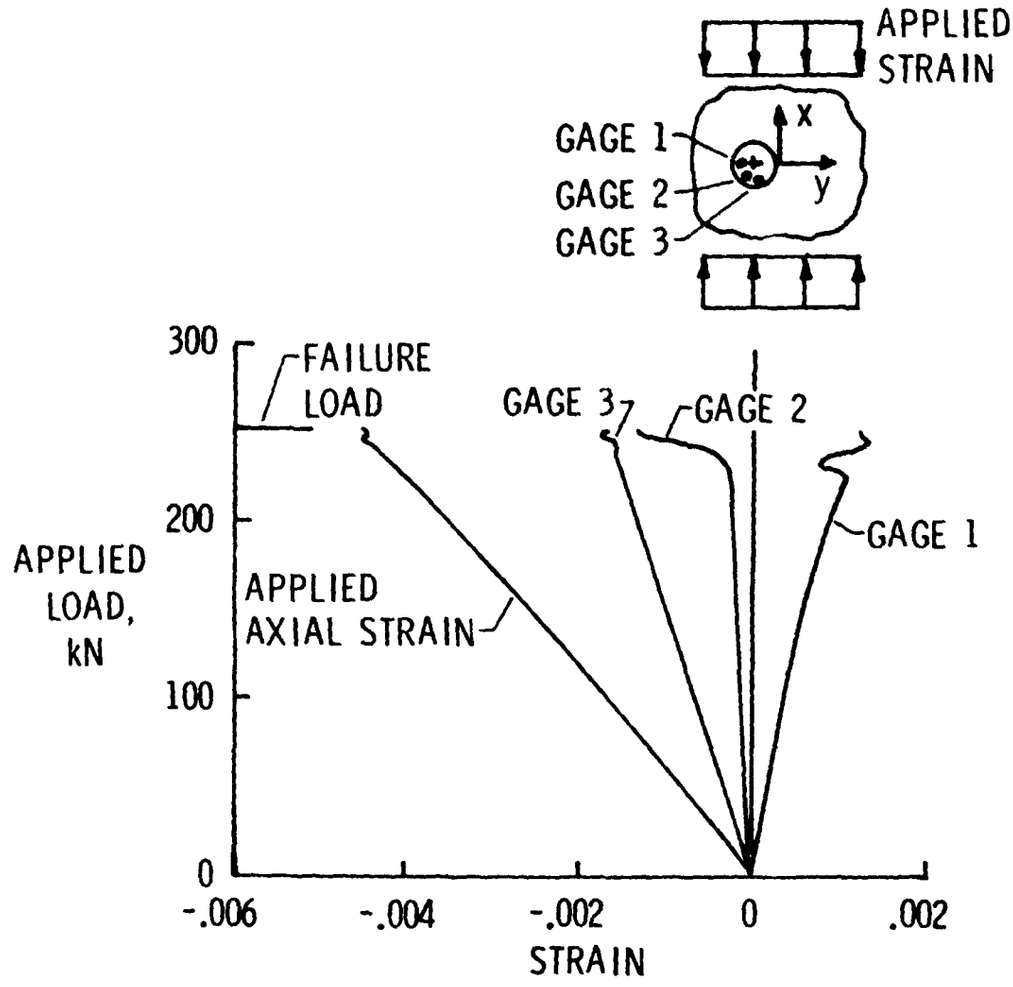


Figure 11.- Interlaminar normal strains at the hole edge for a 1.91 cm diameter hole.

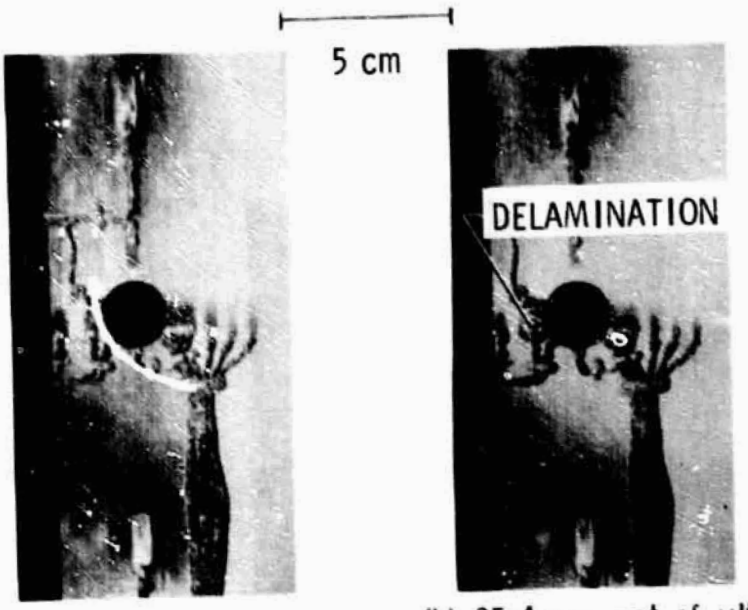


(a) 92.8 percent of ultimate load. No delamination.

(b) 95.4 percent of ultimate load. Delamination to left of hole.

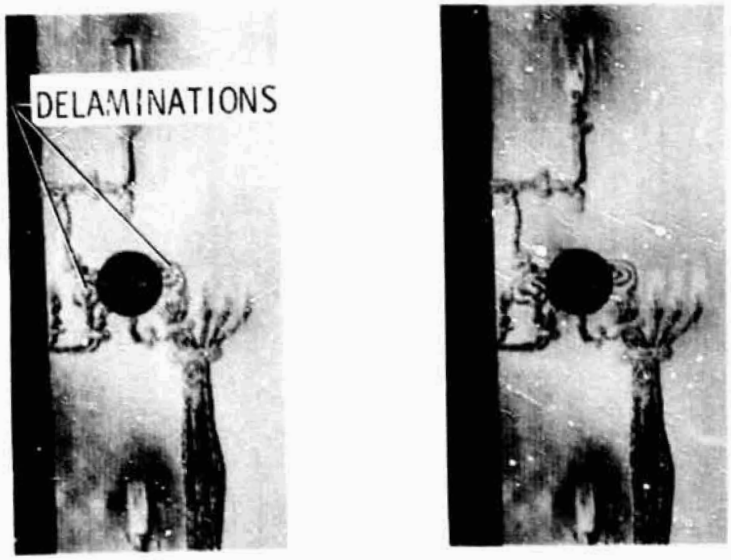


(c) 95.9 percent of ultimate load. Additional delamination to right of hole.

(d) 98.1 percent of ultimate load. Delamination growth.

Figure 12. - Local delamination in hole region and propagation to failure. 1.91 cm diameter hole.

(e) Failed specimen.

Figure 12. - Concluded.

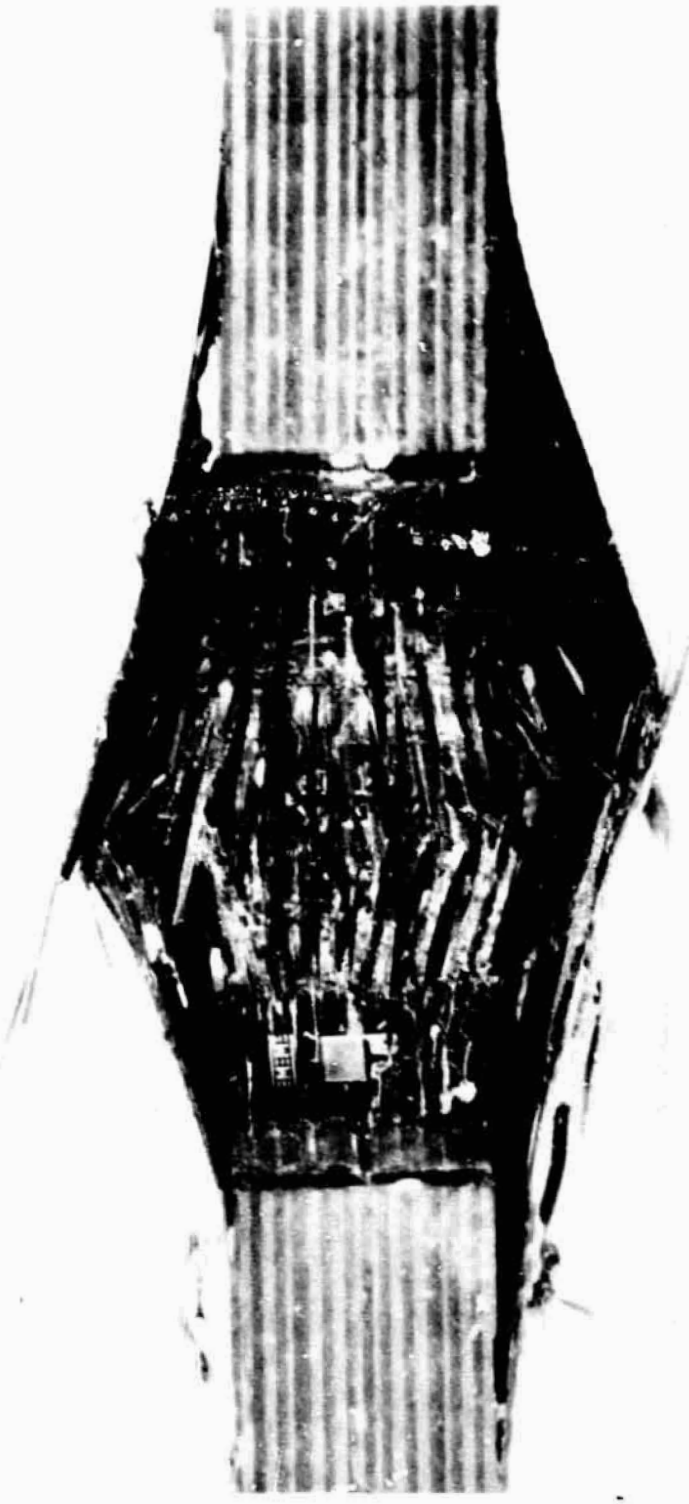



Figure 13. - Cross section of a failed specimen with a 1.91 cm diameter hole.

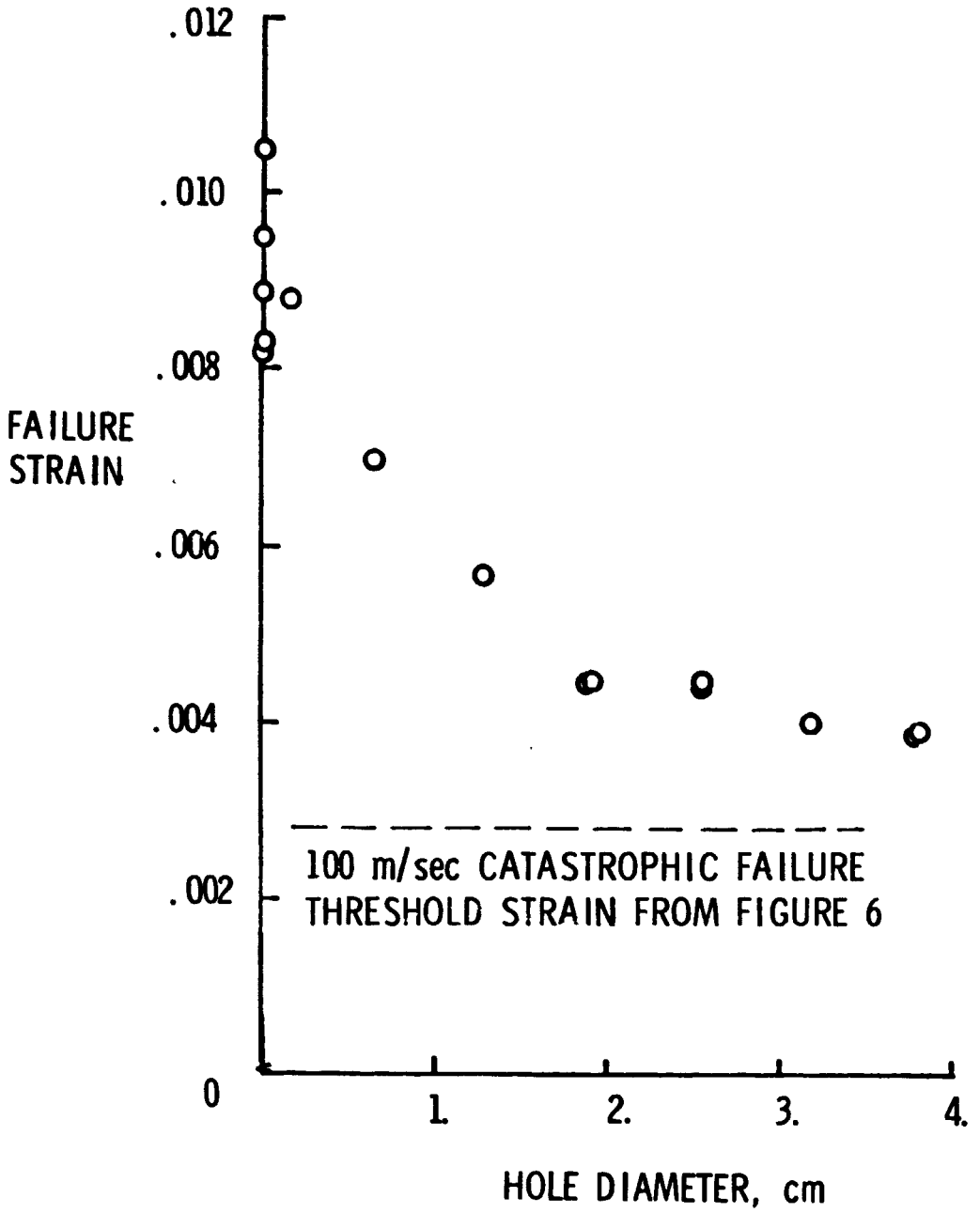


Figure 14. - Effect of hole diameter on laminate compressive strength.

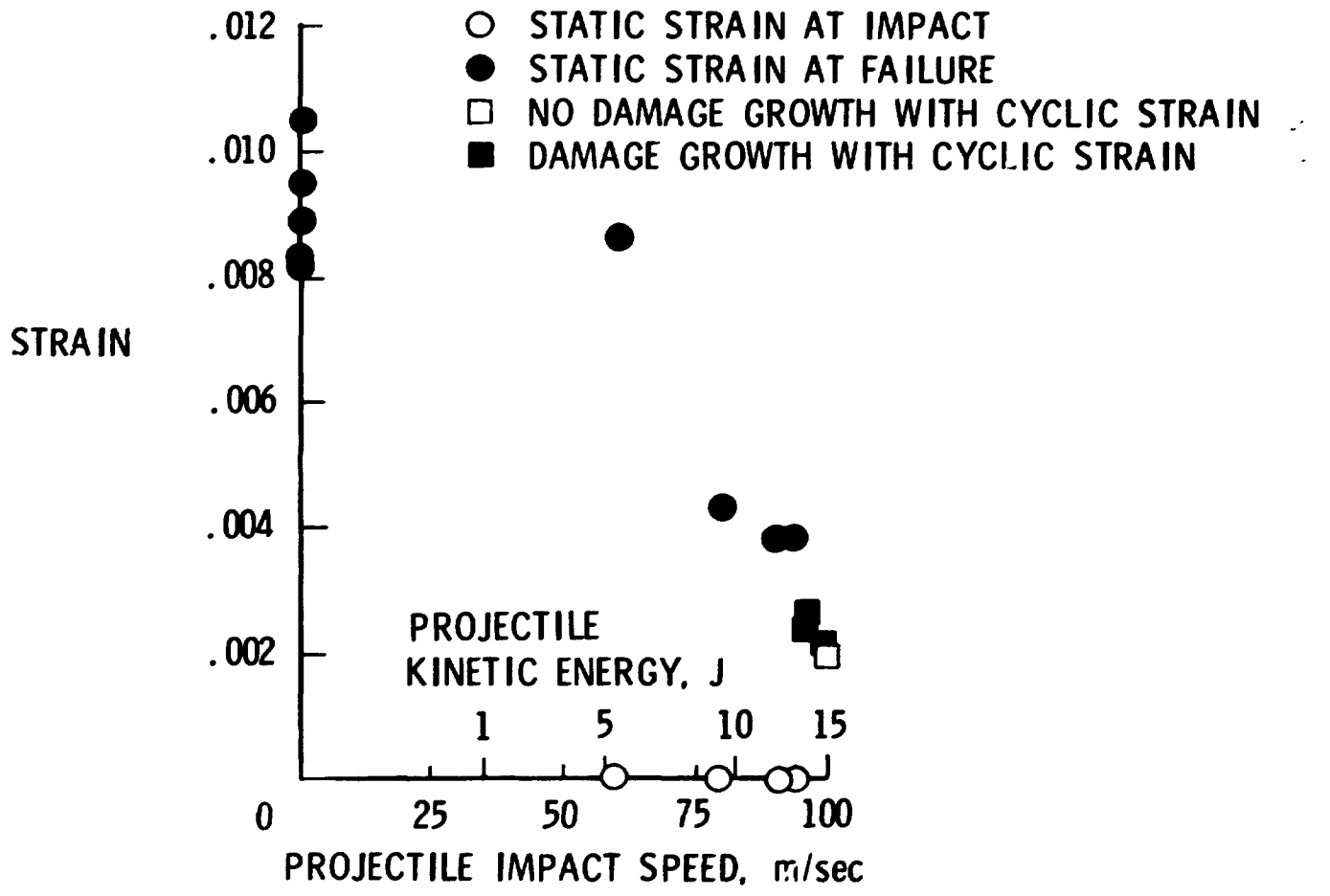


Figure 15. - Effect of cyclic compression-compression loading on the residual strength of impact-damaged specimens.

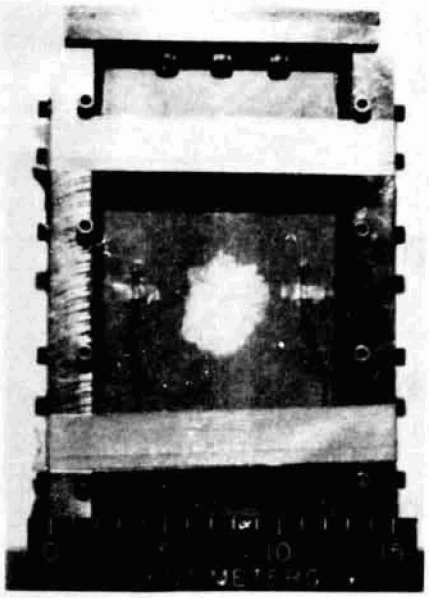

(a) Specimen with initial impact damage.

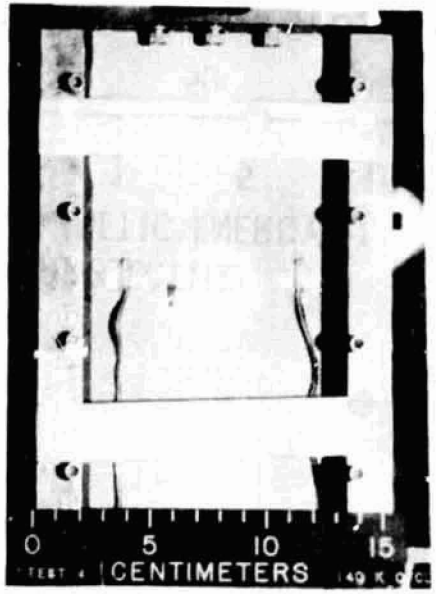


(b) Specimen after 140 000 cycles.

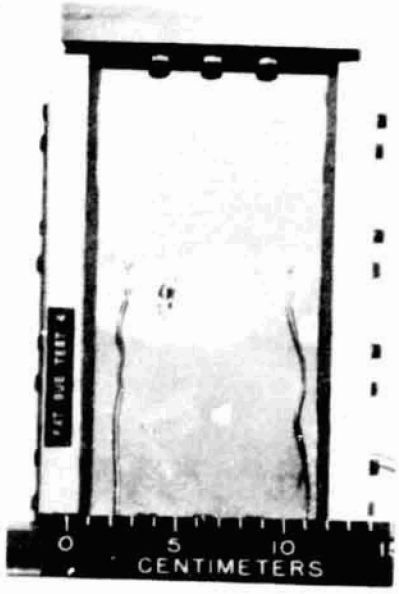


(c) Specimen after failure at 173 000 cycles.

Figure 16. - Effect of cyclic compression-compression loading on a laminate with impact damage. Brittle-lacquer spalling reflects damage growth. Maximum applied axial strain is equal to 0.0025.